Sección de Física
Universidad de La Laguna

THE SVERDRUP BALANCE IN THE EASTERN ATLANTIC

Trabajo de fin de grado realizado por:

Pablo Arteaga Díaz

Bajo la tutorización de:

Pedro Vélez Belchí

y

Teodoro Roca Cortés

La Laguna, Santa Cruz de Tenerife Julio de 2018

CONTENTS

ABSTRACT

Hemos evaluado la validez del llamado balance de Sverdrup en el Atlántico este. Utilizando datos del modelo numérico Oceanic General Circulation Model of the Earth-Simulator (OFES), se calcula el transporte meridional de agua de dos formas distintas: integrando datos de velocidad del modelo numérico (transporte del modelo) y mediante el enfoque teórico del balance de Sverdrup (transporte de Sverdrup), con datos del forzamiento del viento del modelo. El balance de Sverdrup usa el intercambio de momento del viento con la superficie marina como único forzamiento y, por lo tanto, describe los fenómenos cuyo forzamiento principal es el viento. Comparando los transportes del modelo y de Sverdrup, hemos encontrado áreas donde el principal forzamiento no es el viento. Específicamente, nos hemos centrado en una de estas áreas no dominadas por el viento, una banda de aproximadamente 100 km de ancho cerca de la costa africana. Con el análisis del ciclo estacional de los transportes de Sverdrup y del modelo a 30ºN, al lado de la costa africana, hemos identificado la Canary Intermediate Poleward Undercurrent (CIPU), que se sitúa en esa banda, como no dominada por el viento, aunque estos resultados deben ser validados por datos observacionales.

We have assessed the validity of the approach known as the Sverdrup balance in the eastern Atlantic. Using numeric model data from the Oceanic General Circulation Model of the Earth-Simulator (OFES), meridional transport of water is computed in two different ways: integrating velocity data from the numeric model (model transport) and by means of the Sverdrup balance theoretical approach (Sverdrup transport), with the wind-stress model data. The Sverdrup balance is only forced by the wind, and therefore it only describes wind-driven phenomena. By comparing the model and the Sverdrup transports, we have found areas where the main forcing is not the wind. Specifically, we have focused our analysis in one of these areas that are not driven by the wind, a strip of approximately 100 km wide close to the African coast. With the analysis of the model and the Sverdrup transports' seasonal cycle at 30ºN, next to the African coast, we have identified the Canary Intermediate Poleward Undercurrent (CIPU), that is in this strip, as not driven by the winds, although these results should be validated with observational data.

1. INTRODUCTION

En la oceanografía física, la circulación general juega un papel determinante debido a su importancia en el transporte de calor, agua dulce, nutrientes y otros componentes del océano. Particularmente, el transporte meridional, tiene una influencia decisiva en el transporte de calor oceánico, y por ello en el clima global y los ecosistemas marinos. En el océano Atlántico, la Atlantic Meridional Overturning Circulation (AMOC) contribuye al clima del noroeste de Europa, favoreciendo inviernos más suaves que en el noroeste americano a las mismas latitudes. Cambios en la AMOC podrían ocasionar cambios en el clima, por lo que es necesario seguir profundizando en nuestros conocimientos sobre la AMOC, para entender su comportamiento y poder hacer predicciones de posibles variaciones en el futuro. La contribución de este trabajo al conocimiento de la AMOC se hace por medio de la relación teórica entre el intercambio de momento del viento con la superficie oceánica y el transporte meridional, el balance de Sverdrup. El balance de Sverdrup asume que los océanos intercambian momento únicamente con el viento, y esto nos permite utilizarlo como herramienta para identificar fenómenos cuyo principal forzamiento es el viento.

In physical oceanography, general circulation plays a determining role due to its importance in the global transport of heat, fresh water, nutrients and other ocean components. Particularly, meridional transport, or north-south/south-north water transport, plays a determining role in oceanic heat transport, and therefore on the global climate and marine ecosystems. In the Atlantic Ocean, the Atlantic Meridional Overturning Circulation (AMOC) contributes to the north western Europe's mild winters (Seager, et al., 2002). Changes in the AMOC could alter the climate, so it is necessary to study the AMOC in order to understand its behavior and monitor it to make predictions of its possible behavior in the future.

The well-known Sverdrup balance (Sverdrup, 1947) is a theoretical relationship between the momentum transference of the wind to the surface of the ocean (wind-stress) and the meridional transport. From here onwards I will refer to the transport calculated from the Sverdrup balance as *Sverdrup transport*. The Sverdrup balance assumes that the wind is the only stress source, the wind-stress interchanges momentum with the ocean and thus drives the ocean dynamics. It

implies an advantage over other models, because instead of having to introduce velocity measures in full ocean volume, we only need wind measurements on the ocean surface, which we can afford using satellites. Even so, this is not the only utility of the theory: it is also possible to obtain information on which parameters of the ocean dynamics control the different oceanic regimes, comparing its predictions with experimental data. Discrepancies between Sverdrup transport and real transport allows us to find phenomena whose dynamics are not dominated by the wind.

There is a wide variety of studies on the AMOC, although in general its behavior is better known on the western Atlantic than on the east due to historical reasons. Hence, the role of the eastern Atlantic on the meridional transport is still being discussed in the scientific community and it must continue being studied. Recent studies (Velez-Belchí, et al., 2017) have found that the CIPU determines changes in the AMOC: however, the mechanisms of this poleward flow are still unclear.

Unfortunately, there is no enough data to carry out an observational study and as an alternative we can use numeric models. Oceanic numeric models are useful for qualitative analyses, so they could give us information about ocean dynamics. Current numeric models solve numerically the general equations that describe the dynamics of the oceans. Therefore, it is possible to use them to compute transports and consider them as an approximation to reality to understand ocean mechanisms.

In this work, we use oceanic numeric model data together with to the Sverdrup balance theoretical approach to study the dynamics of the CIPU.

2. OBJECTIVES

El propósito de este trabajo es el de ampliar nuestro conocimiento de los mecanismos que dirigen la CIPU. Para lograrlo, estimamos la validez de la teoría de Sverdrup en un área del Atlántico este, lo que nos da información sobre la importancia que el forzamiento del viento tiene sobre la dinámica oceánica y, por lo tanto, sobre la CIPU. Utilizamos datos del modelo numérico OFES (Sasaki, et al., 2008) por un lado, para obtener el transporte meridional del modelo, y por otra parte para obtener el transporte de Sverdrup, y finalmente compararlos. Comparando ambos transportes encontramos las zonas en las que predomina la dinámica de Sverdrup y en las que hay otros mecanismos que la teoría de Sverdrup no considera. Finalmente, usamos esta comparación para determinar la importancia del forzamiento del viento en la dinámica del CIPU por medio del análisis estacional.

The purpose of this work is to expand our knowledge of the mechanisms that drives the CIPU. To achieve that, we estimate the validity of the Sverdrup theory in an area of the eastern Atlantic, which gives us information about the importance that wind forcing has on the ocean dynamics, and therefore, on the CIPU. We use data of the OFES numeric model (Sasaki, et al., 2008) on one hand to obtain the model meridional transport, and on the other, to obtain the Sverdrup transport and finally compare them. Comparing both transports we find the areas where the Sverdrup dynamics predominate and the areas where there are other mechanisms that the Sverdrup theory does not consider. Finally, we use this comparison to determine the wind-stress importance on the CIPU's dynamics by means of the seasonal analysis.

These are the steps we will follow to achieve the above-mentioned objectives:

- To find out the dependence of the Sverdrup transport with the depth.
- To find out the time dependence of the averaged field variables in the Sverdrup transport's accuracy.
- To locate the areas in the eastern Atlantic in which the meridional transport is well described by the Sverdrup transport, as well as the areas which are not.
- To study the seasonal variability of the model and the Sverdrup transport.

3. METHODOLOGY

El transporte meridional promediado a lo largo del tiempo, entre la superficie del mar y una profundidad "d", se puede aproximar mediante el transporte Sverdrup para:

- *Gran escala.*
- *Latitudes medias.*
- *Fluido incompresible.*
- *Teoría de la viscosidad de Boussinesq para el tensor de rozamiento.*
- *Rozamiento horizontal despreciable respecto al vertical.*
- *Asumiendo equilibrio hidrostático en el eje z.*
- *Fluido estacionario.*
- *Aplicando varias restricciones en las condiciones de contorno.*
- *Océano baroclínico.*
- *Asumiendo que el rozamiento solo es introducido por el viento.*

Con la finalidad de identificar si la dinámica de Sverdrup predomina o no en la CIPU, compararemos el trasporte del modelo calculado por medio de la expresión (3-37) y el transporte de Sverdrup por medio de la expresión (3-38) utilizando datos del modelo OFES con resoluciones espaciales de 0.1º en longitudes y latitudes, que son datos de promedios mensuales durante nueve años, desde agosto de 1999 hasta julio de 2009.

3.1 Theoretical background [1]

3.1.1 Momentum equation

Starting from the Eulerian equation of motion that gives the relationship between the field variables ρ (scalar field of density) and $\boldsymbol{V}$ (vector field of velocity) in a fluid. We have an equation equivalent to the principle of linear momentum

[1] The development of this subsection has been extracted from (Schwind, 1980) and (Sverdrup, 1947).

conservation, for geophysical purpose, with reference to a coordinate system fixed to the earth at constant angular velocity $\boldsymbol{\Omega}$:

$$\rho\frac{\partial \boldsymbol{V}}{\partial t}+\rho(\boldsymbol{V}\cdot\boldsymbol{\nabla})\boldsymbol{V}+\rho\boldsymbol{\Omega}x(\boldsymbol{\Omega}x\boldsymbol{r})+2\rho\boldsymbol{\Omega}x\boldsymbol{V}=\boldsymbol{F_v} \qquad (3\text{-}1)$$

where $\boldsymbol{r}=(x,y,z)$, $\boldsymbol{F_v}$ is the net force per unit of volume and it can be expressed in terms of the absolute gravitational potential $-\rho\boldsymbol{\nabla\chi_a}$ and the surface forces per unit volume $\boldsymbol{\nabla}\cdot\wp$.

$$\rho\frac{\partial \boldsymbol{V}}{\partial t}+\rho(\boldsymbol{V}\cdot\boldsymbol{\nabla})\boldsymbol{V}+\rho\boldsymbol{\Omega}x(\boldsymbol{\Omega}x\boldsymbol{r})+2\rho\boldsymbol{\Omega}x\boldsymbol{V}=\boldsymbol{\nabla}\cdot\wp-\rho\boldsymbol{\nabla\chi_a} \qquad (3\text{-}2)$$

Grouping terms:

$$\boldsymbol{g}=-\boldsymbol{\nabla\chi_a}-\boldsymbol{\Omega}x(\boldsymbol{\Omega}x\boldsymbol{r}) \qquad (3\text{-}3)$$

We will take the z axis of our relative coordinate system in the direction of $-\boldsymbol{g}$, the *local down*, the direction of the plumb.

The surface forces per unit volume can be written in terms of pressure $\boldsymbol{p}$ and the viscous stress tensor $\boldsymbol{\tau}$:

$$\rho\frac{\partial \boldsymbol{V}}{\partial t}+\rho(\boldsymbol{V}\cdot\boldsymbol{\nabla})\boldsymbol{V}+2\rho\boldsymbol{\Omega}x\boldsymbol{V}=-\boldsymbol{\nabla}p+\boldsymbol{\nabla}\cdot\boldsymbol{\tau}+\rho\boldsymbol{g} \qquad (3\text{-}4)$$

In order to understand the different terms, making use of the continuity equation

$$\frac{D\rho}{Dt}+\rho\boldsymbol{\nabla}\cdot\boldsymbol{V}=0 \qquad (3\text{-}5)$$

multiplying (3-5) by $\boldsymbol{V}$ and adding the result to (3-4) we obtain:

$$\frac{\partial\rho\boldsymbol{V}}{\partial t}=-\boldsymbol{\nabla}\cdot\rho\boldsymbol{V}\boldsymbol{V}-2\rho\boldsymbol{\Omega}x\boldsymbol{V}-\boldsymbol{\nabla}p+\boldsymbol{\nabla}\cdot\boldsymbol{\tau}+\rho\boldsymbol{g} \qquad (3\text{-}6)$$

where:

- $\frac{\partial\rho\boldsymbol{V}}{\partial t}$ is the local time rate of increase of momentum, per unit volume of fluid.

- $-\boldsymbol{\nabla} \cdot \rho \boldsymbol{V}\boldsymbol{V}$ is the time rate of momentum gain due to advection, per unit volume.
- $-2\rho \boldsymbol{\Omega} x \boldsymbol{V}$ is the time rate of momentum gain due to Coriolis force, per unit volume.
- $-\boldsymbol{\nabla} p$ is the time rate of momentum gain due to the action of pressure force, per unit volume.
- $\boldsymbol{\nabla} \cdot \boldsymbol{\tau}$ is the time rate of momentum gain due to the action of viscous forces, per unit volume.
- $\rho \boldsymbol{g}$ is the time rate of momentum gain due to the action of the gravity, per unit volume.

The focus of the discussion now is the $\boldsymbol{\nabla} \cdot \boldsymbol{\tau}$ factor since it is not easy to describe the viscous stress tensor ($\boldsymbol{\tau} \equiv \tau_{ij}$).

3.1.2 Viscous stress tensor and Navier-Stokes equation

A general form for the viscous stress tensor when there is relative motion between different parts of the fluid and thus internal friction occurs, must meet two conditions. First, it must be dependent on the space derivatives of the velocity, and τ_{ij} cannot contain terms that do not depend on these derivatives since it must vanish for $\boldsymbol{V}$ uniform. And second, τ_{ij} must vanish for uniformly rotating fluids, as there will be no internal friction acting in this kind of motion. According to Eckart (1947), the general expression for τ_{ij} is:

$$\tau_{ij} = \mu \left(\frac{\partial V_i}{\partial x_j} + \frac{\partial V_j}{\partial x_i} \right) + \mu' \delta_{ij} \frac{\partial V_k}{\partial x_k} \qquad (3\text{-}7)$$

where μ and μ' are *dynamic shear* and *bulk* viscosity respectively, and they are not completely independent. Applying the second law of thermodynamic:

$$\frac{\mu}{\rho} \geq 0 \qquad \frac{\mu'}{\rho} \geq -\frac{2}{3}\frac{\mu}{\rho} \qquad (3\text{-}8)$$

The Navier-Stokes expression for τ_{ij} is the limiting case when:

$$\frac{\mu'}{\rho} = -\frac{2}{3}\frac{\mu}{\rho} \qquad (3\text{-}9)$$

This result yields to the Navier-Stokes stress tensor:

$$\tau_{ij} = \mu\left(\frac{\partial V_i}{\partial x_j} + \frac{\partial V_j}{\partial x_i}\right) - \frac{2}{3}\mu\delta_{ij}\frac{\partial V_k}{\partial x_k} \qquad (3\text{-}10)$$

Differentiating it, equation (3-4) becomes the general Navier-Stokes equation:

$$\rho\frac{\partial \boldsymbol{V}}{\partial t} + \rho(\boldsymbol{V}\cdot\boldsymbol{\nabla})\boldsymbol{V} + 2\rho\boldsymbol{\Omega}x\boldsymbol{V} = -\boldsymbol{\nabla}p + \mu\boldsymbol{\nabla}^2\boldsymbol{V} + \frac{1}{3}\mu\boldsymbol{\nabla}(\boldsymbol{\nabla}\cdot\boldsymbol{V}) + \rho\boldsymbol{g} \qquad (3\text{-}11)$$

In physical oceanography, it is often assumed that the fluid is incompressible since it is observed that oceans have almost this behavior. An incompressible fluid means that the field of velocities accomplish that $\boldsymbol{\nabla}\cdot\boldsymbol{V} = 0$, which leads to the result:

$$\frac{\partial \boldsymbol{V}}{\partial t} + (\boldsymbol{V}\cdot\boldsymbol{\nabla})\boldsymbol{V} + 2\boldsymbol{\Omega}x\boldsymbol{V} = -\frac{1}{\rho}\boldsymbol{\nabla}p + \nu\boldsymbol{\nabla}^2\boldsymbol{V} + \boldsymbol{g} \qquad (3\text{-}12)$$

where $\nu = \frac{\mu}{\rho}$ is the *kinematic viscosity*.

3.1.3 Field variables

According to (3-12) we have four independent variables (x, y, z, t), five dependent variables or unknowns (u, v, w, ρ, p) and three equations. In order to have a deterministic set of equations, we need at least two more equations to have five equations and five unknowns, where u, v and w are the meridional, zonal[2] and radial components of the velocity respectively.

Two equations also available are the continuity equation (conservation of mass), which for incompressible flow is:

$$\frac{\partial\rho}{\partial t} + u\frac{\partial\rho}{\partial x} + v\frac{\partial\rho}{\partial y} + w\frac{\partial\rho}{\partial z} = 0 \qquad (3\text{-}13)$$

And the conservation of volume:

$$\frac{\partial u}{\partial x} + \frac{\partial v}{\partial y} + \frac{\partial w}{\partial z} \qquad (3\text{-}14)$$

If incompressibility is not assumed, then we have the three components of the Navier-Stokes equation (3-11) and the continuity equation (3-5). We have four

[2] Longitudinal (west-east) component of velocity.

equations and five independent variables, so it is needed to add another equation, the equation of state:

$$\rho = \rho(s, T, p) \qquad (3\text{-}15)$$

where s is salinity and T is temperature. But the equation of state introduces two more unknowns, then two more equations are needed. By introducing the conservation of salt and the conservation of heat we reach the basic equations of dynamical oceanography. Theoretically, they can be solved if all initial and boundary conditions are given.

3.1.4 Turbulence, statistical treatment and time-averaged equations

In fluid dynamics, turbulence or turbulent flow is characterized by the stochastic behavior of instantaneous velocities. For this reason, a deterministic approach is impossible, so recognizing and analyzing its statistical properties becomes useful.

Ocean dynamics show turbulence, that is, oceans manifest random fluctuations in the velocity field. In practice, we must make measurements of our field variables, but we cannot measure them with accuracy at each point and moment. Therefore, we are more able to study large size and time scale phenomena rather than fine details and small fluctuations on the ocean parameters, and those are the ideas behind the use of the statistical analysis.

Now that the importance of this procedure is understood, we are interested in the mean values of the variables. It will be useful to calculate temporal averages of the fluid dynamics equations that have been previously presented. These averages must be taken over a longer time than turbulence fluctuations and shorter than the fluctuations of the phenomenon we are interested in.

The Reynolds number represents the ratio between inertial forces to the viscous forces:

$$N_R = \frac{LV}{\nu} \qquad (3\text{-}16)$$

where L is the characteristic length, V the characteristic velocity and ν is the kinematic viscosity. Turbulent flow implies high Reynolds number. For regular conditions in large scale ocean dynamics, the characteristic variables are:

Length scale (L)	$\sim 10^6 m$
Horizontal velocity (U, V)	$\sim 1\ m/s$
Vertical velocity (W)	$\sim 10^{-3} m/s$
Depth (H)	$\sim 10^4 m$
Time scale (L/U)	$\sim 10^6 s$
Kinematic viscosity (ν)	$\sim 10^{-3} m^2/s$
Reynolds number (N_R)	$\sim 10^9$

Table 1: Characteristic variables

Averaging over time the momentum equation (3-6) corrected for incompressible fluid, we have the *Reynolds equation for incompressible, turbulent motion*:

$$\frac{D\bar{V}_i}{Dt} + \epsilon_{ijk} f_j \bar{V}_k = -\frac{1}{\rho}\frac{\partial \bar{p}}{\partial x_i} + \frac{\mu}{\rho}\frac{\partial^2 \bar{V}_i}{\partial x_j^2} + g\delta_{i3} - \frac{1}{\rho}\frac{\partial}{\partial x_j}\left(\rho \overline{V_i' V_j'}\right) \qquad (3\text{-}17)$$

where $f = 2\Omega \sin(\varphi)$ (φ is the latitude taken positive to the north of the equator), fw have been neglected due to scale analysis (Table 1), and:

$$\epsilon_{ijk} = \begin{cases} 1\ for\ (i = 2, k = 1) \\ -1\ for\ (i = 1, k = 2) \\ 0\ for\ other\ combinations \end{cases} \qquad (3\text{-}18)$$

It is remarkable that a new term $-(1/\rho)\partial/\partial x_j\left(\rho \overline{V_i' V_j'}\right)$ appears due to the time average, called the *eddy* (or *turbulent* or *Reynolds*) *momentum term* and associated with the turbulent velocity fluctuations.

3.1.5 Reynolds stress and the turbulent coefficients of viscosity

Assuming that each variable is represented by the sum of its mean value plus its fluctuation:

$$V_i = \bar{V}_i + V_i' \qquad (3\text{-}19)$$

and that the mean value of the fluctuation in a long enough period of time is equal to cero ($\bar{V}_i' = 0$) because of its random behavior.

For incompressible laminar flow we had that the stress tensor was $\tau_{ij} = \mu\left(\frac{\partial V_i}{\partial x_j} + \frac{\partial V_j}{\partial x_i}\right)$, and averaging we obtain the *mean viscous stress tensor*:

$$\bar{\tau}_{ij} = \mu\left(\frac{\partial \bar{V}_i}{\partial x_j} + \frac{\partial \bar{V}_j}{\partial x_i}\right) \qquad (3\text{-}20)$$

The term $\tau_{ij}^r = -\rho\overline{V_i' V_j'}$ in the Reynolds equation is called the *Reynolds stress tensor* (it has units of stress, force per unit area), its diagonal components are normal stress and the off-diagonal ones are shear stress. The *total mean stress tensor* can be defined as the sum of the Reynolds stress tensor and the mean viscous stress tensor as the sum of its mean value and a term containing its fluctuations:

$$S_{ij} = \bar{\tau}_{ij} + \tau_{ij}^r = \mu\left(\frac{\partial \bar{V}_i}{\partial x_j} + \frac{\partial \bar{V}_j}{\partial x_i}\right) - \rho\overline{V_i' V_j'} \qquad (3\text{-}21)$$

Despite being a result of great relevance, there are still difficulties to operate mathematically with these expressions. Therefore, some semi-empirical relations have been developed that simplify the stress tensor. We are going to use the Boussinesq's eddy viscosity theory (Boussinesq, 1877) that, in an analogous way of the Newton's viscosity, assumes the Reynolds stress as:

$$\tau_{ij}^r = A_{x_j}\frac{\partial \bar{V}_i}{\partial x_j} \qquad (3\text{-}22)$$

Introducing this term in the Reynolds equation (3-17), assuming differences in A_{x_j} only between horizontal and vertical planes, in three components form we have:

$$\begin{aligned}
&\frac{\partial \bar{u}}{\partial t} + \bar{u}\frac{\partial \bar{u}}{\partial x} + \bar{v}\frac{\partial \bar{u}}{\partial y} + \bar{w}\frac{\partial \bar{u}}{\partial z} - f\bar{v} \\
&\qquad = -\frac{1}{\rho}\frac{\partial \bar{p}}{\partial x} + \frac{1}{\rho}\left[\frac{\partial}{\partial x}\left(A_H\frac{\partial \bar{u}}{\partial x}\right) + \frac{\partial}{\partial y}\left(A_H\frac{\partial \bar{u}}{\partial y}\right) + \frac{\partial}{\partial z}\left(A_V\frac{\partial \bar{u}}{\partial z}\right)\right] \\
&\frac{\partial \bar{v}}{\partial t} + \bar{u}\frac{\partial \bar{v}}{\partial x} + \bar{v}\frac{\partial \bar{v}}{\partial y} + \bar{w}\frac{\partial \bar{v}}{\partial z} + f\bar{u} \\
&\qquad = -\frac{1}{\rho}\frac{\partial \bar{p}}{\partial y} + \frac{1}{\rho}\left[\frac{\partial}{\partial x}\left(A_H\frac{\partial \bar{v}}{\partial x}\right) + \frac{\partial}{\partial y}\left(A_H\frac{\partial \bar{v}}{\partial y}\right) + \frac{\partial}{\partial z}\left(A_V\frac{\partial \bar{v}}{\partial z}\right)\right]
\end{aligned} \qquad (3\text{-}23)$$

$$\frac{\partial \bar{w}}{\partial t} + \bar{u}\frac{\partial \bar{w}}{\partial x} + \bar{v}\frac{\partial \bar{w}}{\partial y} + \bar{w}\frac{\partial \bar{w}}{\partial z} = -\frac{1}{\rho}\frac{\partial \bar{p}}{\partial z} - g + \frac{1}{\rho}\left[\frac{\partial}{\partial x}\left(A_H \frac{\partial \bar{w}}{\partial x}\right) + \frac{\partial}{\partial y}\left(A_H \frac{\partial \bar{w}}{\partial y}\right) + \frac{\partial}{\partial z}\left(A_V \frac{\partial \bar{w}}{\partial z}\right)\right]$$

where A_H and A_V are the horizontal and vertical *turbulence components of the viscosity* respectively.

These equations still have drawbacks due to their complexity, mainly due to the non-linear terms that make them analytically irresolvable and the need to introduce all boundary conditions. However, for certain cases, it is possible to make simplifications that continue describing the system satisfactorily; and this, at the same time, allow us to obtain analytical solutions without requiring a large number of boundary conditions. The Sverdrup balance approximation for meridional transport is an interesting one since it is the fundamental zero-order theory of large-scale circulation (Sverdrup, 1947).

3.1.6 Sverdrup balance

From now on we will omit to denote the variables by their mean values for simplicity, but they should be interpreted as average values.

Making use of scale analysis over the vertical component of the (3-23) equation, for oceanographic, midlatitude, and synoptic scales we can assume: first, that it is possible to neglect the frictional terms; and second, the pressure and gravitational terms are some orders of magnitude larger than the other terms. For Table 1 values, $\theta = 45º \rightarrow f \sim 10^{-4} s^{-1}$ and $\nabla P_z \sim 10^2 dynes/cm^3$:

$\frac{DW}{Dt}$	$2u\Omega\cos(\theta)$	$\frac{1}{\rho}\frac{\partial p}{\partial z}$	g
$\frac{UW}{L}$	fU	$\frac{\nabla P_z}{\rho H}$	g
10^{-7}	10^{-2}	10^{3}	10^{3}

Table 2: Scale analysis

Thus, the behavior of the oceans is very close to hydrostatic equilibrium in the z-axis, so it is possible to compute the pressure, p, at any depth, z, integrating the hydrostatic equation:

$$dp = -\rho g dz \qquad (3\text{-}24)$$

taking into account that the density, ρ, is known from the observations.

The equations of horizontal motion, neglecting the lateral stresses against the vertical (which is known is negligible by scale analysis), are:

$$\frac{\partial u}{\partial t}+u\frac{\partial u}{\partial x}+v\frac{\partial u}{\partial y}+w\frac{\partial u}{\partial z}=-\frac{1}{\rho}\frac{\partial p}{\partial x}+fv+\frac{1}{\rho}\left[\frac{\partial}{\partial z}\left(A_V\frac{\partial u}{\partial z}\right)\right]$$

$$\frac{\partial v}{\partial t}+u\frac{\partial v}{\partial x}+v\frac{\partial v}{\partial y}+w\frac{\partial v}{\partial z}=-\frac{1}{\rho}\frac{\partial p}{\partial y}-fu+\frac{1}{\rho}\left[\frac{\partial}{\partial z}\left(A_V\frac{\partial v}{\partial z}\right)\right] \qquad (3\text{-}25)$$

Considering stationary fluid, which is valid for time averaged values at general circulation scales:

$$\frac{\partial u}{\partial t}=0 \qquad \frac{\partial v}{\partial t}=0 \qquad (3\text{-}26)$$

and neglecting non-linear terms, what means severe restrictions upon the possible lateral boundary conditions., the field accelerations are:

$$u\frac{\partial u}{\partial x}+v\frac{\partial u}{\partial y}+w\frac{\partial u}{\partial z}=0$$

$$u\frac{\partial v}{\partial x}+v\frac{\partial v}{\partial y}+w\frac{\partial v}{\partial z}=0 \qquad (3\text{-}27)$$

Thereby you get to the expressions:

$$\frac{\partial p}{\partial x}=\rho fv+\frac{\partial}{\partial z}\left(A_V\frac{\partial u}{\partial z}\right)$$

$$\frac{\partial p}{\partial y}=-\rho fu+\frac{\partial}{\partial z}\left(A_V\frac{\partial v}{\partial z}\right) \qquad (3\text{-}28)$$

These equations resemble a synthesis of the geostrophic fluid (equilibrium between the pressure gradient and the Coriolis force) and the Ekman wind-driven currents (equilibrium between the wind-stress and the Coriolis force). What combined means that the horizontal pressure gradient is balanced by the Coriolis force and frictional stresses exerted on horizontal surfaces.

In the next step of the original calculation of Sverdrup, the author argues that in homogeneous water the pressure gradient is independent from depth, but that in the case of baroclinic systems (the pressure gradient is due to the slope on the sea surface) depends on the depth. In the ocean, in general cases it can be assumed

that at a certain depth the gradient becomes negligible. This reasoning is important, since in certain low depth areas the argument is not applicable, and therefore the Sverdrup balance is not so useful for some bathymetries.

Following the argument and calling $z = d$ the depth at which the pressure gradient becomes zero, we define two new functions:

$$\frac{\partial P}{\partial x} \equiv \int_d^0 \frac{\partial p}{\partial x} dz \qquad \frac{\partial P}{\partial y} \equiv \int_d^0 \frac{\partial p}{\partial y} dz \qquad (3\text{-}29)$$

Since the horizontal velocity is negligible from $z = d$, the integrals:

$$S_x \equiv \int_d^0 \rho u \, dz \qquad S_y \equiv \int_d^0 \rho v \, dz \qquad (3\text{-}30)$$

represent the components of net mass transport by currents. As boundary conditions it is assumed that the stress is introduces on the surface layer by the wind-stress:

$$\begin{aligned} A_V \frac{\partial u}{\partial z}\Big|_{z=0} &= \tau_x \qquad A_V \frac{\partial u}{\partial z}\Big|_{z=d} = 0 \\ A_V \frac{\partial v}{\partial z}\Big|_{z=0} &= \tau_y \qquad A_V \frac{\partial v}{\partial z}\Big|_{z=d} = 0 \end{aligned} \qquad (3\text{-}31)$$

where τ_x y τ_y are the x and y wind-stress components. Integrating equations (3-28) between $z = d$ and $z = 0$ you get to the equations:

$$\begin{aligned} \frac{\partial P}{\partial x} &= f S_y + \tau_x \\ \frac{\partial P}{\partial y} &= -f S_x + \tau_y \end{aligned} \qquad (3\text{-}32)$$

Making a cross differentiation and subtracting both equations you get:

$$\frac{\partial f}{\partial y} S_y + f\left(\frac{\partial S_x}{\partial x} + \frac{\partial S_y}{\partial y}\right) + \left(\frac{\partial \tau_x}{\partial y} - \frac{\partial \tau_y}{\partial x}\right) = 0 \qquad (3\text{-}33)$$

Furthermore, by integrating the continuity equation knowing that the vertical velocity is zero on the surface and at $z = -d$, we obtain that:

$$\frac{\partial S_x}{\partial x} + \frac{\partial S_y}{\partial y} = 0 \qquad (3\text{-}34)$$

What finally comes to the expression of the Sverdrup balance:

$$\frac{\partial f}{\partial y} S_y + \left(\frac{\partial \tau_x}{\partial y} - \frac{\partial \tau_y}{\partial x} \right) = 0 \qquad (3\text{-}35)$$

Dividing by ρ and rewriting we obtain the Sverdrup curl equation:

$$S_y = \frac{1}{\rho\beta} \hat{\boldsymbol{k}}(\boldsymbol{\nabla x \tau}) \qquad (3\text{-}36)$$

Where $\beta = \frac{\partial f}{\partial y}$, $\hat{\boldsymbol{k}}(\boldsymbol{\nabla x \tau})$ is the z component of the curl of $\boldsymbol{\tau}$,and S_y, the *Sverdrup transport,* is the meridional transport of water volume per unit of time and longitude in the Sverdrup theory.

In summary, the time averaged oceanic meridional transport between the sea surface and a depth d, can be approximated by the Sverdrup transport for:

- Midlatitude and synoptic scales.
- Incompressible flow.
- Boussinesq's eddy viscosity theory for the stress tensor.
- Negligible lateral stress against the vertical one.
- Assuming hydrostatic equilibrium in the z-axis.
- Stationary fluid.
- Applying several restrictions to the boundary conditions.
- Baroclinic ocean.
- Assuming that stress is only introduced by the wind.

Under these assumptions, we can conclude that the wind is the main parameter that controls oceanic motion at large scale meridional mass transports. It is a useful insight to sea modeling in a simple way in which the only boundary conditions needed are relatively easy to measure by satellites, so we can ask ourselves whether these results are fulfilled in practice, and whether the Sverdrup balance, in fact, describes the ocean dynamics. If there are other forcings rather than wind, the Sverdrup balance will not be fulfilled. In this case, we will verify

where the Sverdrup balance, the geostrophic balance in the presence of the wind, is fulfilled in the Eastern Atlantic to determine if CIPU is a wind-driven current.

3.2 Data

We use numeric model data because the velocity is not usually measured. Hence, when using measurement data, we are forced to introduce some approximations to obtain transports. Geostrophic approximation is often used. In addition to that, there are no measurements with such spatial resolution and for as long periods of time as the model data. Model data can be approximated to reality, and specifically, in the study area Romero García et al. (2016) have proven that OFES numeric model reproduces the ocean dynamics.

We use velocity data from the OFES numerical model, and the wind-stress that forces OFES model. All the data is stored in the *GDS* OPeNDAP Server of the *Asia-Pacific Data Research Center (APDRC)* (APDRC, n.d.). OFES has simulations forced by the wind with NCEP and QuickSCAT data. QuickSCAT has better spatial resolution with small scale structures and this is the reason why it has been used instead of NCEP wind forced data.

OFES model has monthly mean and three-days mean data. Monthly mean data is used because results were equal to monthly mean and it would have taken a greater cost in computing time. Moreover, Sverdrup theory describes long time averaged data and not short time fluctuations, as it was stated in the theoretical approach and as it is going to be shown later.

The magnitudes of the spatial and temporal resolutions of the model are below the magnitudes of the characteristic variables shown in Table 1. Therefore, the model fulfills the resolution requirements to describe the phenomena we are interested in.

The studied area ranges from 0-30^{o} W, 20-40^{o} N, and from August 1999 to July 2009. First months of the available data were omitted because the QuickSCAT satellite was not in orbit, and last month was omitted in order to take exact years and avoid seasonal phenomena impact on time averages.

3.2.1 Velocity data

Monthly mean meridional velocity data is generated by OFES making use of their numeric model. It is stored in a 4-D matrix (longitudes, latitudes, depths and times) with the following grid dimensions:

- Longitudes: from 0.1^{o} to 360.0^{o} E given with 0.1^{o} resolution.
- Latitudes: from -74.9^{o} N to 75.0^{o} N given with 0.1^{o} resolution.
- Depths: from 2.50000 mb to 5900.00000 mb given by levels with 111.27358 mb resolution.
- Times: from January 1999 to September 2009 with monthly resolution.

3.2.2 Wind-stress data

We use the wind-stress data that forces the model for the computations of the Sverdrup transport. Monthly mean wind-stress data is provided by OFES and stored in a 3-D matrix (longitudes, latitudes and times) with the following grid dimensions:

- Longitudes: from 0.1^{o} to 360.0^{o} E given with 0.1^{o} resolution.
- Latitudes: from -74.9^{o} N to 75.0^{o} N given with 0.1^{o} resolution.
- Times: from January 1999 to September 2009 with monthly resolution.

The wind stress used by OFES is not exactly that of the QuickSCAT satellite (Figure 1), it has been resampled to its grid (with 0.1^{o} spatial resolution) and constructed by weighted mean method (Kutsuwada, 1998), as Sasaki et al. (2006) stated. As it can be observed in Figure 1,there are some small scales features of the actual wind-stress curl that are filtered out in the model forcing. According to Risien & Chelton (2008), as a result of antenna sidelobe contamination,

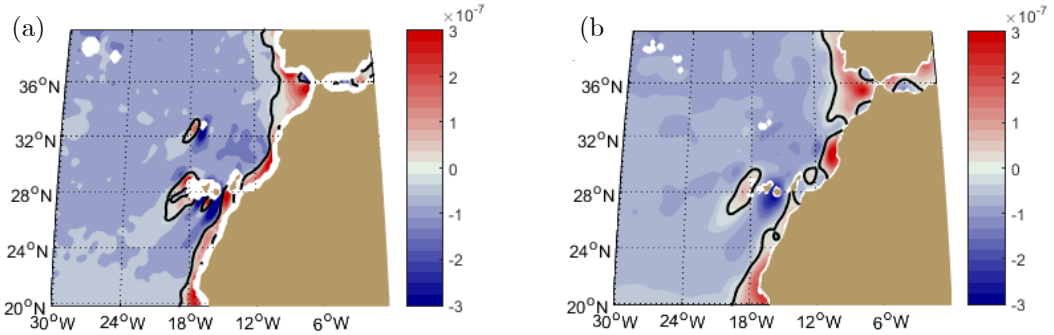

Figure 1: Eigth-year average of the wind-stress curl in N/m^2 per meter. Image (a) represents QuickSCAT data from the Scatterometer Climatology of Ocean Winds (SCOW) (Risien & Chelton, 2008) and image (b) represents QuickSCAT data of the OFES model.

standard QuikSCAT measurements cannot be obtained closer than about 30 km to land. The OFES model generates those values to compute its simulations.

3.3 Physical magnitudes and computations

3.3.1 Meridional transport

Using meridional velocity data, the meridional transport of water volume, per unit of time, at a given latitude, between longitudes l_1 and l_2 is:

$$T = \int_d^0 \int_{l_1}^{l_2} \bar{v}\, dxdz \qquad (3\text{-}37)$$

The depth limit $z = d$, at which the momentum exchange between the wind and the ocean can be considered negligible. The choice of the depth d is not clear since it is not a constant in the oceans, but we will discuss this topic in 4.2.

Using wind-stress data in the Sverdrup curl equation (3-36), the meridional transport of water volume, per unit of time, at a given latitude, between longitudes l_1 and l_2 is:

$$S = \int_{l_1}^{l_2} \frac{1}{\rho\beta}\left(\frac{\partial \bar{\tau}_x}{\partial y} - \frac{\partial \bar{\tau}_y}{\partial x}\right) dx \qquad (3\text{-}38)$$

Where $\bar{v}$, $\bar{\tau}_x$ and $\bar{\tau}_y$ are time averaged values over a certain time that we are going to discuss in 4.3. In our case, these integrals are numerical integrals, then it is necessary to choose an integration method; we use the composite trapezoidal rule. Meridional transport is going to be expressed in Sverdrup units ($1\ \mathrm{Sv} = 10^6\ \mathrm{m^3/s}$).

4. RESULTS AND DISCUSSION

Haciendo un análisis de la validez del balance de Sverdrup en el Atlántico este, mediante una comparación del transporte de Sverdrup con el transporte del modelo, obtenemos como resultado que existe una franja de alrededor de 100 km junto a la costa africana en la que los resultados del transporte de Sverdrup no reproducen los del modelo. Por esta zona pasan dos corrientes: la CUC y la CIPU. Mediante el análisis del ciclo estacional en la zona cercana a la costa, conociendo el ciclo estacional de la CIPU con un máximo en otoño, observamos su influencia, con ese máximo en otoño, en el ciclo estacional del transporte del modelo. Por otra parte, no se encuentra esa influencia en el del transporte de Sverdrup. Este hecho nos lleva a pensar que, dado que el balance de Sverdrup no predice la dinámica de la CIPU, la CIPU no está forzada por el viento.

4.1 Velocity and wind-stress fields

The western Atlantic velocity field in the analysis area is mainly characterized by the Canary Current and the Azores Current as it can be seen in Figure 2-a. According to most studies, the Azores Current branches from the Gulf towards the east. In Figure 2-a it can be seen entering from the east at latitude 35^{o}N and passing through the archipelago of the Azores. The Canary Current is a wide branch of the North Atlantic Current that flows southward parallel to the European and the African western coasts, it is a wind-driven surface current. It can be seen in Figure 2-a from the west coast of the Iberian Peninsula, parallel to the African coast and passing through the Canary Islands. Although not shown in Figure 2-a, the current joins the Atlantic North Equatorial Current. In addition to the Canary Current, along the African coast there are two other currents, the Canary Upwelling Current (CUC) (Figure 2-a) and Canary Intermediate Poleward Undercurrent (CIPU) (Figure 2-b). The CUC flows southward, and it is a costal upwelling current. The CIPU has a maximum of transport around 800 m depth and goes from south to north, in the opposite direction to the other currents.

The wind is characterized by the Azores high with low wind-stress near Azores and higher stress as the distance to the center of the high increases (Figure 2-c).

Next to the Iberian Peninsula and the African coast, the wind-stress decreases again, thus changing the curl sign, as Figure 1-b shows.

Differences between velocity and wind-stress fields give us an insight of the differences between Sverdrup and model transports.

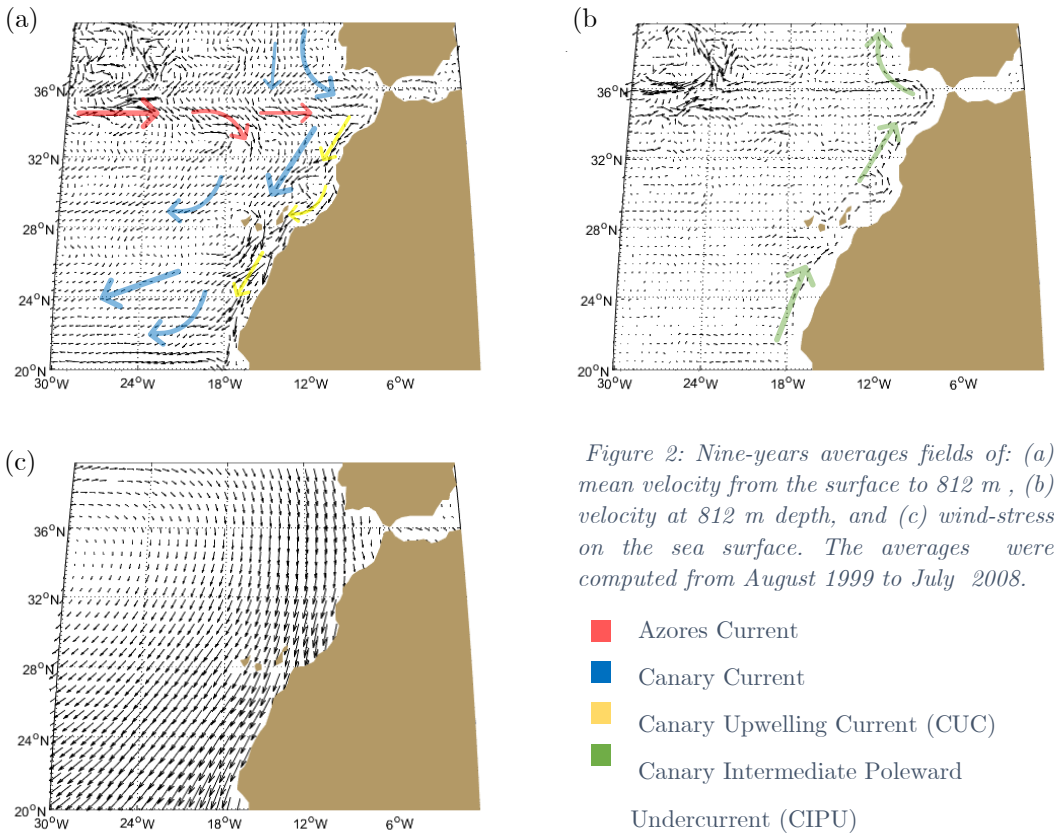

Figure 2: Nine-years averages fields of: (a) mean velocity from the surface to 812 m , (b) velocity at 812 m depth, and (c) wind-stress on the sea surface. The averages were computed from August 1999 to July 2008.

4.2 Vertical dependence of the Sverdrup Balance with the integration depth

It was seen in the theoretical section 3.1.6 that the Sverdrup transport is the transport between the sea surface and a depth d in which the wind-stress effect on the ocean dynamics becomes negligible. The problem now is to find that depth. According to Wunsch (2011), a possible method is looking for the depth in which the vertical velocity $w(d)$ satisfy $|w(d)| < 10^{-8}\, m/s$, what turns out to be an arbitrary choice. In order to find the dependence of the Sverdrup balance with the integration depth, our approach is to define a new parameter, $\eta(d)$, as:

$$\eta(\mathrm{d}) = \sum_{ij} \left(T_{ij}(d) - S_{ij}\right)^2 \qquad (4\text{-}1)$$

where the summation is over every longitudes and latitudes (i, j) of the model grid. $T_{ij}(d)$ corresponds to equation (3-37) integrating T to a depth d in 0.1^{o} longitude sections at each grid point (i, j), and S_{ij} to equation (3-38) integrating in 0.1^{o} longitude sections for each grid point (i, j). T and S are computed with $\bar{v}$, $\bar{\tau}_x$ and $\bar{\tau}_y$ averaged over nine years (from August 1999 to July 2008). The parameter $\eta(\mathrm{d})$ gives us an idea of the accuracy of the Sverdrup transport with the integration depth over the whole area. In Figure 3, we can see that it is almost constant in the first meters, decreasing from $50.7\ Sv^2$ on the surface to a minimum of $32.8\ Sv^2$ at $\mathrm{d} = 293\ \mathrm{m}$ and increasing to $65.5\ Sv^2$ at 812 m.

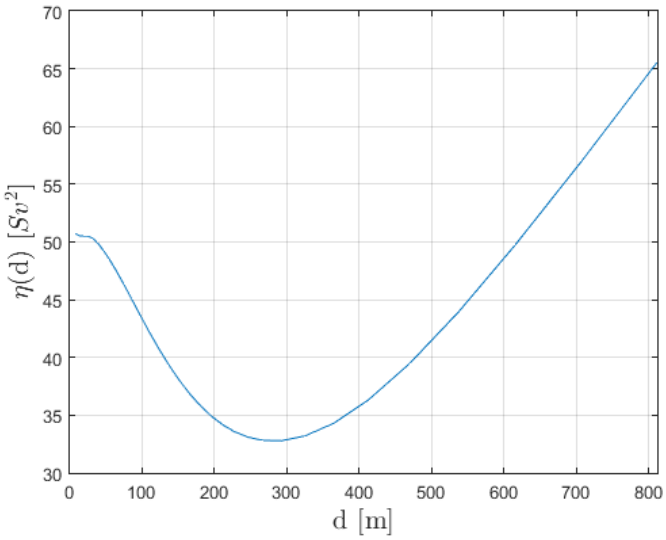

Figure 3: Vertical dependence of the Sverdrup balance with the integration depth. Horizontal axis represents depths in meters and vertical axis $\eta(d)$, equation (4-1), in square Sverdrup units [Sv^2].

However, in this case, we are interested in a current, the CIPU, that has its maximum transport around $800\ m$ depth (Romero García, et al., 2016), so we will use $d = 812\ m$ (the nearest depth to $800\ m$ that is available in the model grid) for the integrations of the model transport T (3-37). For this depth, the ocean dynamics are not as accurately defined by the Sverdrup balance as for $\mathrm{d} = 293\ \mathrm{m}$. We are aware that we are introducing some errors due to this integration depth, since our main objective is not to verify the Sverdrup balance, but to use it as a tool to identify the mechanisms of oceanic phenomena. Moreover, calculations of the model transport with $\mathrm{d} = 293\ \mathrm{m}$ are not too different from

those with $\mathbf{d = 812\ m}$, being a softened version with lower transports and thus being more like the Sverdrup transport.

4.3 Dependence on the accuracy of the Sverdrup balance with temporal averages

In order to study the statistical properties of the ocean dynamics, time averages of the field variables where introduced in 3.1.4. It was stated that it was necessary to carry out time averages during enough time to remove the stochastic behavior of the turbulence, but it was not specified how much was "enough time".

In the same way we did in 4.2, we will define other two parameters, $\sigma(t)$ and $\sigma(\Delta t)$, for the estimation of the time dependence of the Sverdrup balance:

$$\sigma(t) = \sum_{ij} \left(T_{ij}(t) - S_{ij}(t)\right)^2 \qquad (4\text{-}2)$$

$$\sigma(\Delta t) = \sum_{ij} \left(T_{ij}(\Delta t) - S_{ij}(\Delta t)\right)^2 \qquad (4\text{-}3)$$

where the summations are over every longitudes and latitudes (i, j) of the model grid. T_{ij} corresponds to equation (3-37) integrating T in 0.1^{o} longitude sections at each grid point (i, j), and S_{ij} to equation (3-38) integrating in 0.1^{o} longitude sections for each grid point (i, j). $T_{ij}(t)$ and $S_{ij}(t)$ are computed with $\bar{v}$, $\bar{\tau}_x$ and

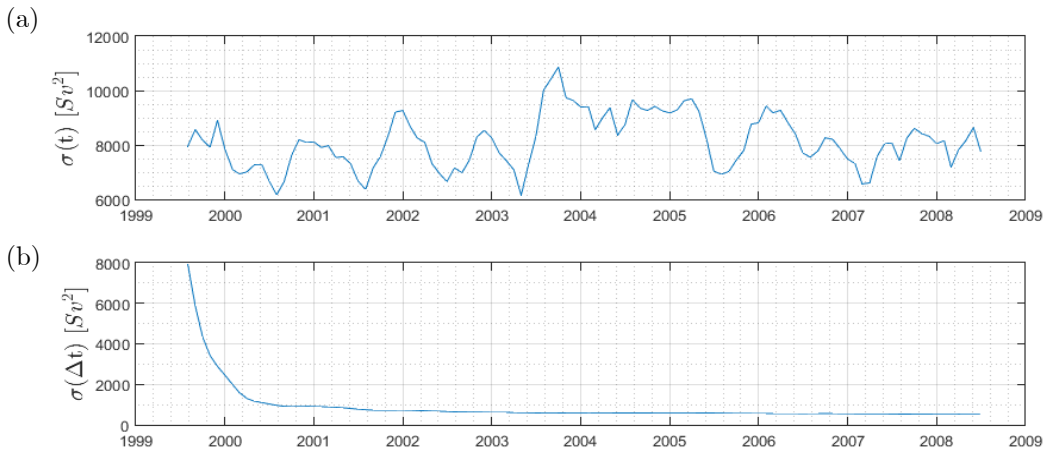

Figure 4: Dependence on the accuracy of the Sverdrup transport with the time average of the field variables. Image (a) represents the monthly mean error ($\sigma(t) = \sum_{ij}\left(T_{ij}(t) - S_{ij}(t)\right)^2$), and image (b) the error as a function of the average time (Δt) for the field variables ($\sigma(\Delta t) = \sum_{ij}\left(T_{ij}(\Delta t) - S_{ij}(\Delta t)\right)^2$).

$\bar{\tau}_y$ monthly means, and $T_{ij}(\Delta t)$ and $S_{ij}(\Delta t)$ are computed with $\bar{v}$, $\bar{\tau}_x$ and $\bar{\tau}_y$ averaged from August 1999 to a date Δt later. The parameter $\sigma(t)$ gives us an idea of the error of the Sverdrup transport at each month, while $\sigma(\Delta t)$ represents the error of the Sverdrup transport for the field variables averaged over a time Δt. Figure 4 shows how for apparent "random" errors $\sigma(t)$ taking different monthly averages (Figure 4-a), the error $\sigma(\Delta t)$ decreases for longer time averages (Figure 4-b).

A year average can be considered enough time (Δt), as it is seen in Figure 4-b, for a reduction of the error $\sigma(\Delta t)$ in one order of magnitude, since it decays from $7950\ Sv^2$ to $950\ Sv^2$ in a year. For seasonal averages (three months averages), $\sigma(\Delta t)$ decreases from $7950\ Sv^2$ to $4340\ Sv^2$, so Sverdrup transport is less accurate for seasonal averages of the field variables than for annual or interannual averages. After a nine-year average, the error $\sigma(\Delta t)$ decays to $550\ Sv^2$

Another remarkable thing from this analysis is that the errors $\sigma(t)$ are not entirely random, since it is seen that the error is usually higher autumn and winter and lower in spring and summer (Figure 4-a) due to some seasonally variable phenomena that introduces error. This topic will be developed in more in the seasonal analysis.

It has been stated how accurate the results of the Sverdrup transport are in function of the time-averages of the field variables, and it has turned out that it is not as accurate for monthly or seasonal analysis as for interannual ones.

4.4 Differences between the Sverdrup transport and the model transport

Following the main objectives of this work, we look for differences between the model and the Sverdrup transport. In Figure 5 it is shown the model transport T (3-37) (Figure 5-a) and the Sverdrup transport S (3-38) (Figure 5-b). The model transport is characterized by southward transport in most of the area, with some local northward maxima next to Azores and southward transport maxima around Azores, Madeira and Canary archipelagos. It shows small scale phenomena that Sverdrup transport does not. Sverdrup transport is characterized by southward transport in most of the area like model transport, and northward in

the eastern part of the area, next to the African coast. It has some local northward, and southward maxima near the Canary Islands. The Sverdrup northward transport next to the African coast does not match with the southward flow of the CUC, which means that the Sverdrup balance is not capable of reproducing it. The CUC current is due to the effect of the wind near the coast, what causes an upwelling of depth cold water producing a pressure gradient as result. This kind of wind-driven phenomena are not reproduced by the Sverdrup balance because of its time variability of the order of days.

In general, the Sverdrup transport (Figure 5-b) is a smoothed version of the model transport (Figure 5-a) with some differentiated areas next to the continental coasts and near the Azores and Madeira Islands (most remarkable in Azores, which are not treated in this work).

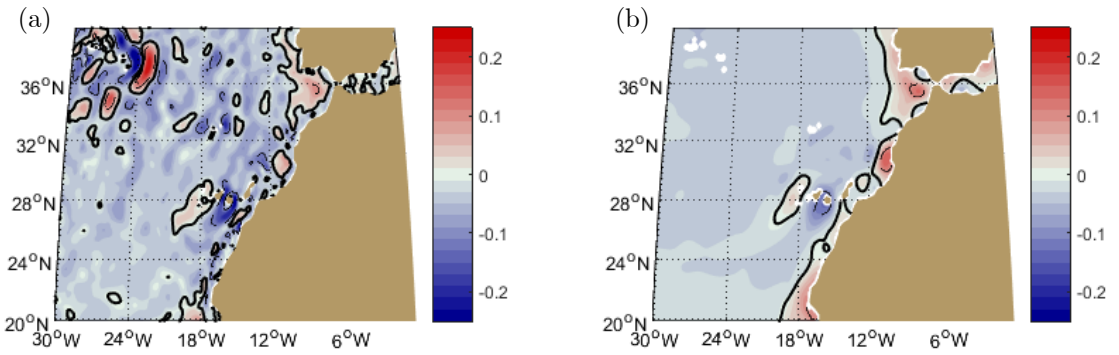

Figure 5: Meridional transport maps. The image (a) correspond to the model transport T (3-37) and the image (b) correspond to the Sverdrup transport S (3-38) with velocities and wind-stresses averaged over nine years. The colours represent meridional transport per unit of time, at each latitude, in a 0.1º longitude width in Sverdrup units [Sv] ($1\,Sv = 10^6\,m^3/s$). Solid lines are $0\,Sv$ lines, and discontinue lines are at $-0.1\,Sv$ and $0.1\,Sv$.

In order to quantify differences between model and Sverdrup transport, let's define Δ as the difference between T and S:

$$\Delta = T - S \qquad (4\text{-}4)$$

where T is the model transport (3-37) and S the Sverdrup transport (3-38).

In most of the area, the parameter Δ is between $-0.1\,Sv$ and $0.1\,Sv$ (Figure 3 discontinue lines mark $-0.1\,Sv$ and $0.1\,Sv$), so Sverdrup and model transport coincide with differences of an order of magnitude less than $10^{-1}\,Sv$, in 0.1º longitude width sections. There are small differences characterized by positive and negative values of Δ in contiguous areas that becomes more important in shorter

time-averages (Figure 8). Figure 6 shows that the biggest differences between T and S are in a strip of ~100 km width next to the African coast line as it is also seen in Figure 5, and next to Azores, but we are interested in the African coast area, in which the CIPU is located. The areas of higher Δ values next to the African continent match with the areas where de CUC and the CIPU are located, since Sverdrup transport is to the north while model transport is to the south, being the Sverdrup balance unable to reproduce the behavior of the CUC, which predominates in the area.

Our results in Figure 5 and Figure 6 are coherent with those of Gray & Riser (2014), but with a higher spatial resolution, showing that the differences between the Sverdrup balance transport and the modelled transport are in a strip of ~100km width close to the African coast.

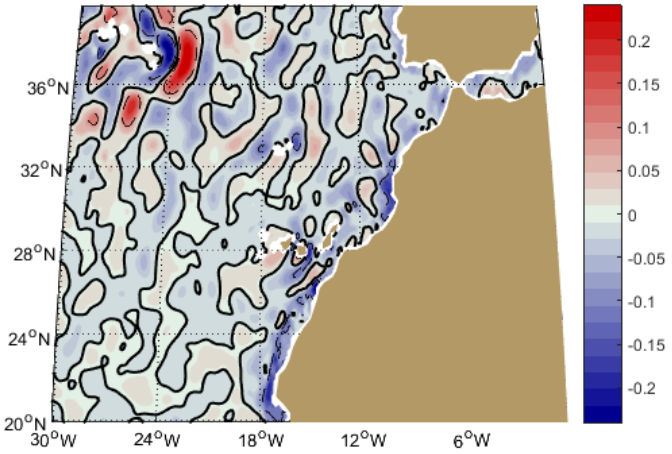

Figure 6: Transport differences map of $\Delta = T - S$. Where the model transport T is computed by the integral (3-37) and the Sverdrup transport S by (3-38) with velocities and wind-stresses averaged over nine years. The colours represent meridional transport per unit of time, at each latitude, in a 0.1º longitude width in Sverdrup units [Sv] ($1\,Sv = 10^6\,m^3/s$). The solid line is located at $0\,Sv$, and discontinue lines are at $-0.1\,Sv$ and $0.1\,Sv$.

The statistic distribution of the Δ values in the analysis area gives us more precise information on the accuracy of the Sverdrup transport, since 96% of the values are between -0.1 Sv and 0.1 Sv, 33% between -0.01 Sv and 0.01 Sv and 3% between -0.001 Sv and 0.001 Sv. The parameter Δ is then characterized by the Figure 6-c in a quantitative way. The maximum and minimum values in Figure 7-a, b and c are ($0.24\,Sv$, $-0.30\,Sv$), ($0.15\,Sv$, $-0.13\,Sv$) and ($0.28\,Sv$, $-0.27\,Sv$) respectively. And the mean values in Figure 7-a, b and c are $-0.032\,Sv$, $-0.026\,Sv$ and $-0.007\,Sv$ respectively.

The statistical distribution of the model transport (Figure 7-a) is wider than the Sverdrup transport (Figure 7-b) in concordance with Figure 5, in which Sverdrup transport is a smoothed version of the model transport. Sverdrup transport's distribution is not symmetric, since it has more weight in the positive part (red areas of northward transport in Figure 5-b, next to the African coast), and it can be seen in Figure 7-c (statistical distribution of Δ) that contribution of the Sverdrup transport in the negative part (since $\Delta = T - S$).

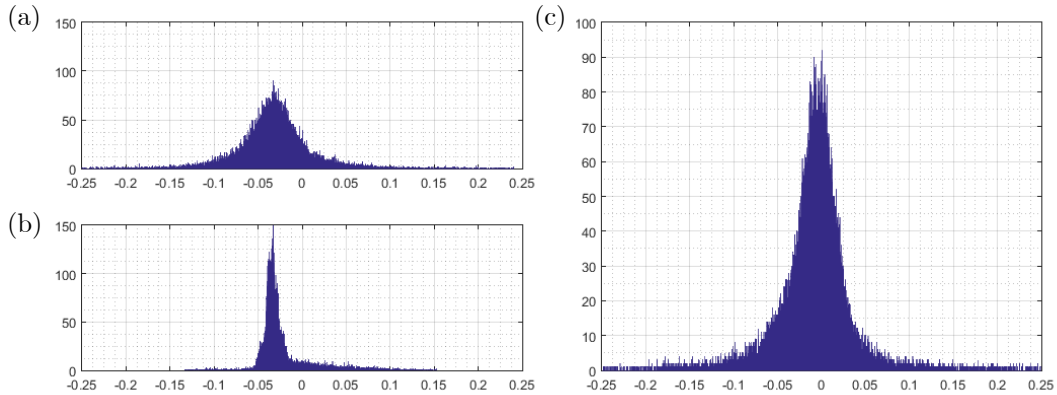

Figure 7: Histograms of the values in Figure 5-a (a), Figure 5-b (b) and Figure 6 (c) taking 5000 bins between -0.25 *and* $0.25\ Sv$.

4.5 Seasonal variability

We have focused on the interannual average of the difference between Sverdrup transport and model transport. Now we will analyze the seasonal variation of this difference. We will centre on the African coasts, where we can study the mechanisms of the CIPU, and the differences between model and Sverdrup transport are bigger. For simplicity, seasons have been taken as: winter (January, February, March), spring (April, May, June), summer (July, August, September) and autumn (October, November, December).

For seasonal averages (Figure 8), turbulent behaviour of the ocean becomes more visible than for interannual ones (Figure 6), then there are more differences between the model transport and the Sverdrup transport, as seen in Figure 4-b.

Making a seasonal analysis of the meridional transport, it is observed that the Sverdrup transport in the African coasts is closer to the transport of the model in autumn, i.e. the difference between T and S, Δ , is lower in this season. In Figure 8, the mean seasonal Δ maps are shown for winter (Figure 8-a), spring (Figure 8-

b), summer (Figure 8-c) and autumn (Figure 8-d). It can be appreciated that the differences next to the African coast are smaller in autumn (light-blue areas next to the African coasts in Figure 8-d) than in the other seasons (dark-blue areas next to the African coasts in Figure 8-a, b and c). However, this result is not coherent with the fact that the CIPU has a maximum of northward transport in the autumn season. Therefore, we will do a more quantitative analysis, studying the seasonal variability at 30ºN in 5º longitudinal regions from the African coast to 30ºW. We have chosen 30ºN section because it is a region close to the Canary Islands which is usually monitored, and it is not influenced by the effect of the islands and the interruption of the southward flow of the Canary current.

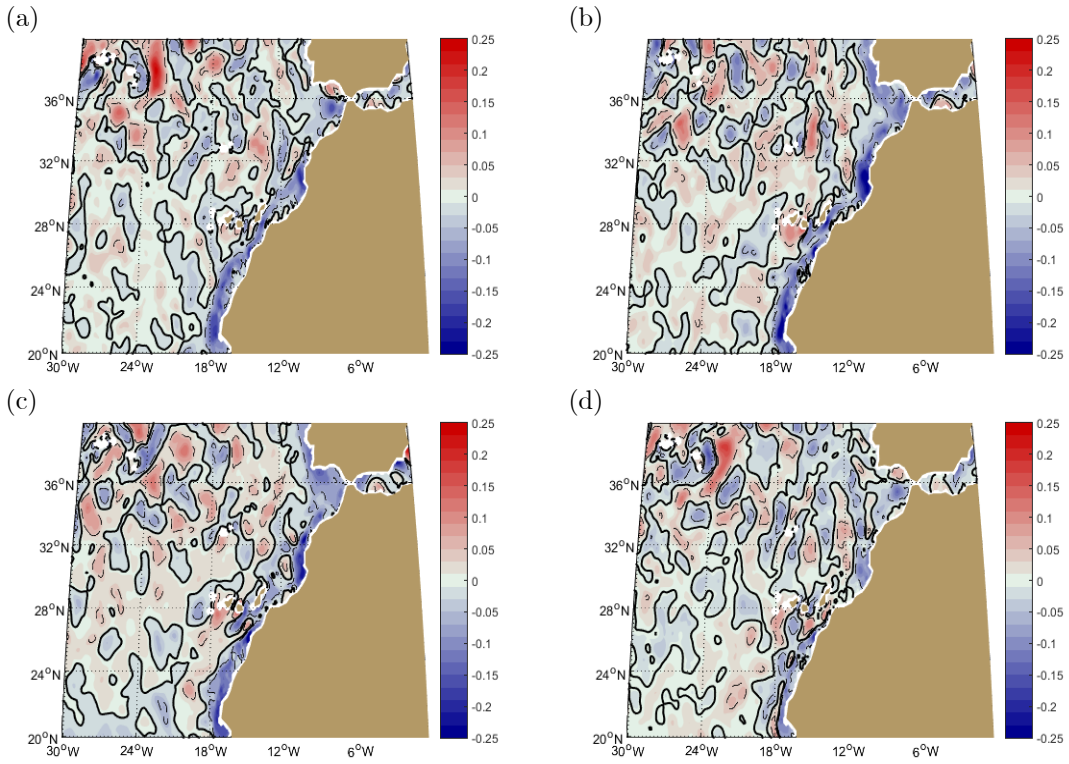

Figure 8: Seasonal maps of $\Delta = T - S$*, where the model transport T is computed by the integral (3-37) and the Sverdrup transport S by (3-38) with velocities and wind-stresses seasonally averaged over nine years. The colours represent meridional transport per unit of time, at each latitude, in a 0.1º longitude width in Sverdrup unit [Sv] (*$1\,Sv = 10^6\,m^3/s$*). Solid lines are* $0\,Sv$ *lines, and discontinue lines are at* $-0.05\,Sv$ *and* $0.05\,Sv$*. Images (a), (b), (c) and (d) are winter, spring, summer and autumn respectively.*

In the three sections farthest from the African coast (Figure 9-a, Figure 9-b and Figure 9-c), the transports T (3-37) and S (3-38) are similar, with differences between $0\,Sv$ and $2\,Sv$ ($0.2\,Sv$, $0.6\,Sv$ and $0.3\,Sv$ mean differences in Figure 9-a, b and c respectively). However, in the section closer to the African coast (Figure 9-d), the differences between transports T and S are higher throughout the year than in the sections farther from the coast line, ranging between $2\,Sv$ and $6\,Sv$, with $3.9\ Sv$ as the mean difference, which is one order of magnitude higher than

the mean differences in the other sections. In this 10ºW-15ºW section, Sverdrup transport is towards the north, whereas model transport is towards the south, this being in line with Figure 6. T and S are closer to each other in autumn season, with differences around $2\,Sv$ (Figure 9-c). This lower Δ values in autumn are caused by the CIPU, since the Canary current and the CUC have southward flow, and CIPU has northward flow with its maximum of transport in autumn season. In autumn, the transport of the model approaches zero when adding the southward flow of the Canary Current and the CUC with the maximum northward flow of the CIPU, and thus it is closer to the Sverdrup transport (Figure 9-d). As this increase of the northward transport in the autumn season is appreciable in the seasonal cycle of the model transport but not in that of the Sverdrup transport, the Sverdrup balance is unable to explain CIPU's contribution to the meridional transport. Therefore, CIPU's mechanisms must be forced by other forcing instead of wind. Figure 9-d agrees with Romero García et al. (2010) results of the seasonal cycle of the velocities next to the African coast with model and observational data at 800 m depth, where the CIPU predominates in the contribution to meridional transport.

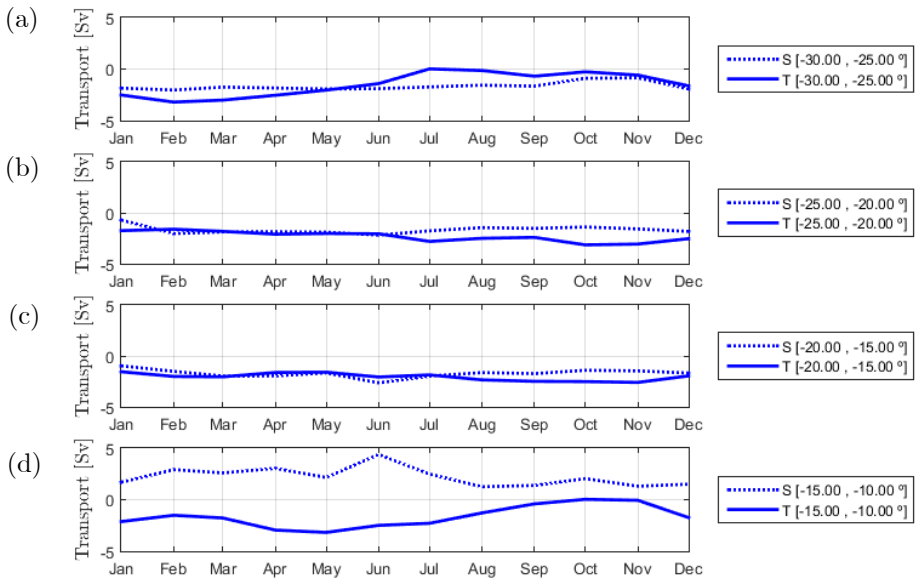

Figure 9: Seasonal cycle of the meridional transport at 30º N between 30º W and 25º W in image (a), between 25º W and 20º W in image (b), between 20º W and 15º W in image (c) and between 15º W and 10º W in image (d); all in Sverdrup units [Sv] ($1\,Sv = 10^6\,m^3/s$). Solid lines represents model transport T (3-37) and discontinued lines the Sverdrup transport S (3-38) with velocities and wind-stresses seasonally averaged over nine years.

Integrating the transport over the whole 30ºN section, from the African coast to 30ºW, we obtain Figure 10, where the mean difference between model and Sverdrup transport is $2.9\,Sv$. This offset between T and S transports is caused

mainly by the differences between T and S close to the African coast. Neglecting the offset, the differences in the seasonal cycles are higher in August, September and January, especially in September before the characteristic peak in October-November.

It is interesting to point out that this estimation of the Sverdrup transport (Figure 10) agrees with the estimations of Kanzow (2010) for the seasonal cycle of the eastern boundary contribution to the midocean section of the overturning strength of the AMOC. This seasonal cycle is characterized by a sharp peak of transport in October-November, with a considerable increase of transport between September and October, in the same way as Sverdrup transport in Figure 10. Kanzow's calculations were made from moorings data, applying the geostrophic approximation, and the Sverdrup balance corresponds to the geostrophic balance in the presence of the wind. It is possible that mooring data in the eastern boundary of the Atlantic are not showing ocean real behavior due to the use of the geostrophic approximation. Because of that, their seasonal cycle is more like the Sverdrup transport than the model transport, which takes into account more dynamics and forcing than the geostrophic approximation.

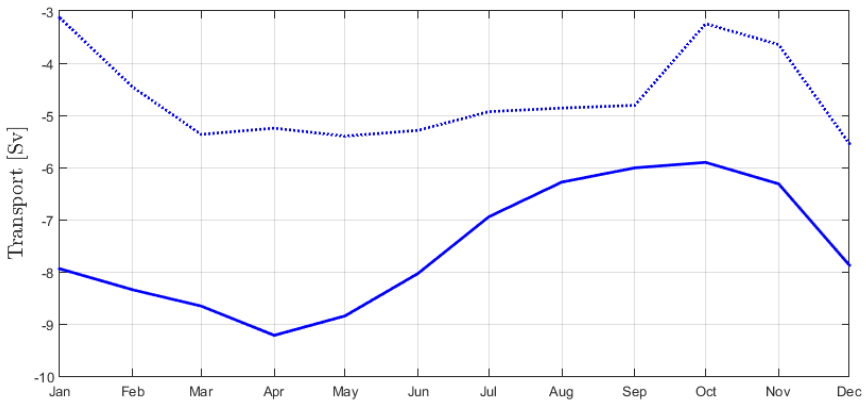

Figure 10: Seasonal cycle of the meridional transport at $30^{o}N$ between $30^{o}W$ and $10^{o}W$ in Sverdrup units [Sv] ($1\,Sv = 10^{6}\,m^{3}/s$). Solid lines represents model transport T (3-37) and discontinued lines the Sverdrup transport S (3-38) with velocities and wind-stresses seasonally averaged over nine years.

5. CONCLUSIONS

En este trabajo, hemos utilizado el balance de Sverdrup como una herramienta para estudiar los mecanismos oceánicos en el Atlántico este, utilizando datos del modelo oceánico OFES. Específicamente, hemos utilizado este enfoque para estudiar la Canary Intermediate Poleward Undercurrent (CIPU), ya que suponíamos que no estaba forzada por el viento. Como los efectos de la CIPU en el ciclo estacional del transporte meridional están presentes en el ciclo estacional del transporte del modelo, pero no en el del transporte de Sverdrup, los resultados muestran que la dinámica de la CIPU no está forzada por el viento. Quedan por estudiar los mecanismos oceánicos que fuerzan la CIPU, y por qué el ciclo estacional observado por Kanzow (2010) se parece más al ciclo estacional del transporte de Sverdrup que a las simulaciones del modelo.

In this work, we have assessed the Sverdrup balance in the eastern Atlantic, using oceanic model data as a tool to study ocean mechanisms. Specifically, we have used this approach to study the Canary Intermediate Poleward Undercurrent (CIPU), since we hypothesize that it is not driven by the wind forcing. We have used OFES model data due to the fact that it has been demonstrated that it describes properly the ocean circulation in the eastern Atlantic. This study is limited to the use of model data because there are not enough data from moorings and buoys to carry out an observational study.

The horizontal distribution of the Sverdrup transport and the differences between model meridional transport and the Sverdrup meridional transport are in concordance with those of Gray & Riser (2014), although our higher resolution results show that the differences between the Sverdrup balance transport and the modelled transport are in a strip of ~100km width close to the African coast. Although the Sverdrup balance is closer to the modelled transport over longer times and using $\mathsf{d} = 293\ \mathsf{m}$ as the integration depth. Calculations were made with an integration depth of $\mathsf{d} = 812\ \mathsf{m}$, the depth at which the CIPU's transport has a maximum, since our focus was on the CIPU. As the effects of the CIPU in the meridional transport's seasonal cycle are present in the seasonal cycle of the model transport, but not in that of the Sverdrup transport, the results show that CIPU's dynamics are not forced by the wind. It remains to study the oceanic mechanisms that force the CIPU, and why the seasonal cycle observed by Kanzow (2010) is

similar to the seasonal cycle from the Sverdrup transport rather than from the model simulations. It is also on the agenda to make an observational validation of our results.

The methodology used here could be used to study non-forced by the wind phenomena around the Azores. Although the Sverdrup balance is a very useful tool, it is a fairly simplified ocean theoretical model, it would be possible to use more complex models to carry out this type of analysis. Understanding the mechanisms that drive meridional water transport in the eastern Atlantic allows us to adequately carry on observational studies in the future, in order to continue expanding our knowledge about the transport of heat, nutrients, oxygen, etc. in a more detailed way in the area.

BIBLIOGRAPHY

APDRC, n.d. *Asia-Pacific Data-Research Center (APDRC).* [Online] Available at: http://apdrc.soest.hawaii.edu/tutorials/opendap.php [Accessed 11 May 2017].

Boussinesq, J., 1877. *Essai sur la théorie des eaux courantes.* Paris: Impr. nationale (Paris).

Eckart, C., 1947. *Excerpts of notes on Scripps Institute of Oceanography Course 217.* La Jolla: Unpublished.

Gray, A. R. & Riser, S. C., 2014. A Global Analysis of Sverdrup Balance Using Absolute Geostrophic Velocities from Argo. *Journal Of Physical Oceanography,* 44(4), pp. 1213-1229.

Kanzow, T. y otros, 2010. Seasonal Variability of the Atlantic Meridional Overturning Circulation at 26.58N. *Journal of Climate,* Volumen 23, pp. 5678-5698.

Kutsuwada, K., 1998. Impact of wind/wind-stress field in the North Pacific constructed by ADEOS/ NSCAT data. *Journal of Oceanography,* Volumen 54, p. 443–456.

NASA, n.d. *Winds, Measuring Ocean Winds from Space.* [Online] Available at: https://winds.jpl.nasa.gov/missions/quikscat/ [Accessed 15 February 2018].

Pond, S. & Pickard, G. L., 2007. *Introductory Dynamical Oceanography.* Oxford: Butterworth-Heinemann.

Risien, C. & Chelton, D., 2008. A Global Climatology of Surface Wind and Wind Stress Fields from Eight Years of QuikSCAT Scatterometer Data. *Journal of Physical Oceanography,* Volumen 38, pp. 2379-2413.

Romero García, E., Vélez Belchí, P., Sánchez Leal, R. & Hernández Guerra, A., 2016. *The Canary Deep Poleward Undercurrent.* Alicante, España: V Simposio

Internacional de Ciencias del Mar - Encuentro de la Oceanografía Física Española 2016.

Sasaki, et al., 2008. An eddy-resolving hindcast simulation of the quasiglobal ocean from 1950 to 2003 on the Earth Simulator. In: K. H. a. W. O. (eds.), ed. *High Resolution Numerical Modelling of the Atmosphere and Ocean.* New York: Springer, pp. 157-185.

Sasaki, H. y otros, 2006. An Eddy-Resolving Simulation of the Quasi-Global Ocean Driven by Satellite-Observed Wind Field. *Journal of the Earth Simulator,* Volumen 6, pp. 35-49.

Schwind, J. J. v., 1980. *Geophysical Fluid Dynamics for Oceanographers.* Second ed. Englewood Cliffs: Prentice-Hall.

Seager, R. y otros, 2002. Is the Gulf Stream responsible for Europe's mild winters?. *Q.J.R. Meteorol. Soc.,* 128(586), p. 2563–2586.

Sverdrup, H., 1947. Wind-driven currents in a baroclinic ocean; with application to the equatorial currents of the eastern Pacific. *Proc Natl Acad Sci USA,* 33(11), p. 318–326.

Velez-Belchí, P. et al., 2017. On the seasonal variability of the Canary Current and the Atlantic Meridional Overturning Circulation. *Journal of Geophysical Research: Oceans,* 122(6), p. 4518–4538.

Wunsch, C., 2011. The decadal mean ocean circulation and Sverdrup balance. *Journal of Marine Research,* 69(2), pp. 417-434.